

Hydrogenation of CO₂ to methanol over Au–CuO/SBA-15 catalysts

Yanyan Li^{1,2} · Wei Na^{1,3} · Hua Wang^{1,3} · Wengui Gao^{1,3}

Published online: 6 October 2016
© Springer Science+Business Media New York 2016

Abstract A series of Au–CuO/SBA-15 catalysts with 1–3 wt% Au and 30 wt% CuO were successfully prepared for CO₂ hydrogenation to methanol by chemical reduction and the following impregnation. The influence of Au content on the physicochemical properties of Au–CuO/SBA-15 catalysts was investigated in terms of ICP-AES, N₂ physisorption, XRD, TEM, N₂O titration, XPS and H₂–TPR technique. The results showed that the as-prepared Au–CuO/SBA-15 catalysts exhibited higher catalytic activity than CuO/SBA-15 catalyst. 2 % Au–CuO/SBA-15 catalyst showed the best catalytic activity with 13.5 % methanol selectivity and 24.2 % CO₂ conversion for CO₂ hydrogenation to methanol. The addition of Au NPs played an important role in improving the catalytic activity for CO₂ hydrogenation to methanol, which may be attributed to the interaction between Au and CuO.

Keywords Au–CuO/SBA-15 catalysts · CO₂ hydrogenation · Methanol · Au/CuO interaction

Electronic supplementary material The online version of this article (doi:10.1007/s10934-016-0295-8) contains supplementary material, which is available to authorized users.

✉ Wei Na
weina@kmust.edu.cn

- ¹ State Key Laboratory of Complex Nonferrous Metal Resources Clean Utilization Engineering, Kunming University of Science and Technology, Kunming 650093, China
- ² Faculty of Chemical Engineering, Kunming University of Science and Technology, Kunming 650093, China
- ³ Faculty of Metallurgy and Energy Engineering, Kunming University of Science and Technology, Kunming 650093, China

1 Introduction

It is well known that global warming problems become more and more serious due to the gradual increase of anthropogenic CO₂ concentration in the atmosphere [1, 2]. CO₂ is also regarded as an important carbon source due to its plenty, inexpensive and nontoxic. In this context, the utilization of CO₂ to synthesis chemicals and fuels has attracted more attention for the excellent benefits to both environment and economy. Up to now, CO₂ hydrogenation to methanol has been considered as one of the effective and economical ways to fix and utilize the emitted CO₂ (CO₂ + 3H₂ = CH₃OH + H₂O, ΔH_o = –49.8 kJ mol^{–1}). It is mainly because that methanol is not only an important chemical intermediate to produce some chemicals such as formaldehyde and acetic acid, but also an excellent fuel due to its cleaner emissions in comparison with other fossil fuels [3–5]. The new concept of “Methanol Economy”, proposed by Olah’s group, was based on the great significance of CO₂ hydrogenation to methanol [6].

Industrial methanol was produced from synthesis gas (CO + H₂) on ternary catalyst Cu–ZnO–Al₂O₃ at high pressure (~10 MPa). However, it was a pity that the catalytic performance of ternary catalyst Cu–ZnO–Al₂O₃ for CO₂ hydrogenation to methanol was not satisfied due to the negative effect of large amounts of water from the reverse gas shift reaction (RWGS, CO₂ + H₂ = CO + H₂O, ΔH_o = 41.2 kJ mol^{–1}) in the presence of the hydrophilic alumina carrier [7]. To further enhance the catalytic performance, numerous efforts have been devoted to developing effective catalysts for CO₂ hydrogenation to methanol during the past several decades. For example, Cu–Zn–Al–Zr system was extensively studied for this purpose [8, 9]. In addition, the influence of different promoters such as La, Ce, CaO and TiO₂ on the catalytic

performance of Cu-based catalysts have been also widely investigated [10–12]. These conventional strategies can indeed improve the catalytic performance of Cu-based catalysts to some degree, but fail to overcome the obstacles about the insufficiency of the adsorption-dissociation hydrogen and deactivation owing to the sintering and agglomeration of CuO nanoparticles (NPs) with lower BET surface area at high temperature [13]. Therefore, this observation hinted that we should pursue a better strategy to solve the issues as much as possible.

Recently, it has been reported that some Au-containing catalysts were more active than Cu-based catalysts for methanol synthesis from CO₂ hydrogenation [14–17]. It was reported that higher methanol yield was obtained by using Au/ZnO/TiO₂ catalyst with smaller Au particles [18]. The reason can be attributed to an increase in Au–ZnO interfaces. Although Au is expensive, previous researchers have indicated that the promising potential of Au for small scale operation under dynamic operation conditions and the positive effect of Au on the catalytic performance for CO₂ hydrogenation to methanol has been stressed [14]. Moreover, it has been found that the first subgroup B (IB) elements (such as Au and Cu) could produce strong interaction or form alloy with each other since they possessed similar face center cubic crystal structure and lattice spacing.

In addition to the compositions, preparation methods and pretreatment conditions, the support materials of catalysts also have considerable influences on the catalytic activity. Mesoporous material especially SBA-15 mesoporous molecular sieve was regarded as a promising support because of its unique merits such as highly ordered two-dimensional hexagonal mesoporous structure, large specific surface area, controllable pore size and thick pore wall. Especially, the large specific surface area and mesoporous structure can improve the dispersion of active sites in catalyst and provide nano-sized, uniform reaction environments which enable to stabilize small metal or metal oxide NPs inside mesopores [19]. For example, highly dispersed Cu NPs on Cu/SBA-15 provided abundant active sites and thus led an efficient performance in WGS reaction [20]. Homogeneous dispersion of Au NPs into SBA-15 also improved the catalytic activity for nitroaromatic [21]. Liu et al. [22] developed a two-step method to prepare well-dispersed Au–Ag alloy NPs on MCM-41 and Au–Cu alloy NPs on SBA-15, which also exhibited a high activity for CO oxidation. However, there are few researches that involved the influence of Au content on the catalytic activity of Cu-based catalysts supported by SBA-15 with respect to CO₂ hydrogenation to methanol reaction at present.

In this work, a series of Au/SBA-15 with 1–3 wt% Au were successfully prepared by the adsorption of chloroauric

acid onto the NH₂–SBA-15 and the following chemical reduction by NaBH₄. Then, 30 wt% CuO was loaded by the impregnation method. In order to examine the structure–activity relationship of Au/CuO–SBA-15, the as-prepared catalysts were also characterized by ICP-AES, N₂ physisorption, XRD, TEM, N₂O titration, XPS and H₂–TPR technique, and the corresponding catalytic activity of the as-prepared catalysts was also evaluated for CO₂ hydrogenation to methanol reaction.

2 Experimental

2.1 Materials

Pluronic123 (triblock copolymer EO₂₀PO₇₀EO₂₀), tetraethoxysilane (TEOS) and 3-Aminopropyltriethoxysilane (APTES) were purchased from Sigma Aldrich. Hydrogen tetrachloroaurate (HAuCl₄·3H₂O), copper nitrate (Cu(NO₃)₂·3H₂O) and sodium borohydride (NaBH₄) were obtained from Aladdin. All reagents were used without further purification.

2.2 Catalyst preparation

2.2.1 Preparation of SBA-15

Mesoporous silica SBA-15 was synthesized via the method proposed by Zhao et al. [23]. At 40°C, 7.5 g Pluronic123 was dissolved in 240 mL 2 M HCl aqueous solution under stirring for 4 h. Then, 20 mL TEOS were added dropwise under stirring and then kept for 24 h at 40°C. The obtained suspension was transferred into polyethylene bottles and kept for another 48 h at 100°C without stirring. After the hydrothermal treatment, the sample was filtered, washed several times with deionized water and then dried at 60°C for 24 h. Finally, the dried sample was calcined at 550°C for 6 h to remove the template.

2.2.2 Grafting of APTES on the surface of SBA-15

In a 500 mL round-bottom flask, 4.0 g SBA-15 was dissolved in 300 mL ethanol containing 12 mL APTES, and the mixture was then refluxed at 85°C for 24 h. The sample (denoted as NH₂–SBA-15) was collected by filtration, washed with ethanol several times and then dried at 60°C for 24 h.

2.2.3 Preparation of Au–CuO/SBA-15

A series of Au–CuO/SBA-15 catalysts with 1–3 wt% Au and 30 wt% CuO were successfully prepared by a two-step process. The Au/SBA-15 was prepared by chemical

reduction method, using HAuCl_4 (98 wt%) as the source of Au. At 25°C, 1.5 g $\text{NH}_2\text{-SBA-15}$ was mixed with a required amount of 0.0025 M HAuCl_4 aqueous solution under stirring for 40 min, followed by adding a required amount of 0.1 M NaBH_4 aqueous solution under ultrasonic for 20 min. After the suspension was filtered, washed with deionized water and then dried at 60°C for 24 h, $\text{Au/NH}_2\text{-SBA-15}$ was obtained. Then, the obtained $\text{Au/NH}_2\text{-SBA-15}$ was calcined at 350°C for 3 h.

The Au-CuO/SBA-15 catalyst was prepared by impregnation method. At 40°C, the resultant $\text{Au/NH}_2\text{-SBA-15}$ was dissolved in 0.02 M $\text{Cu}(\text{NO}_3)_2$ aqueous solution under stirring for 3 h. Then, the mixed solution was filtered, washed with deionized water and then dried at 60°C for 24 h. Finally, Au-CuO/SBA-15 catalyst was obtained after the dried mixture was calcined at 350°C for 5 h.

2.3 Characterization of catalyst

The actual Au and Cu loadings of the as-prepared catalysts were determined by ICP-AES (Vista-MPX, Varian). The specific surface areas and pore volume were determined from N_2 adsorption–desorption (Autosorb-iQ, Quantachrome) at -196°C . The as-prepared catalysts were treated with degassing at 300°C for 10 h before the adsorption. BET method was utilized for the evaluation of adsorption isotherms. XRD (D/max RC diffractometer, Rigaku) was performed with a $\text{Cu K}\alpha$ radiation at 40 kV from 0° to 10° (the scan rate: $2^\circ/\text{min}$) and $20^\circ\text{--}80^\circ$ (the scan rate: $8^\circ/\text{min}$). The crystallite size was calculated based on the Debye–Scherrer formula:

$$D = \frac{K\lambda}{\beta \cos \theta}$$

where K is a constant (taken as 0.94), λ is the wavelength ($\lambda = 0.154$ nm for $\text{Cu-K}\alpha$ X-rays) and β is the full width at half maximum (FWHM) [24]. The morphology and structure of the sample were probed by TEM (JEM-2100, JEOL). The particle size distribution was calculated by measuring more than 100 particles from arbitrarily selected different areas. The metallic copper surface area (S_{Cu}) and dispersion (D_{Cu}) were determined by dissociating N_2O adsorption [25]. XPS (PHI5000 Versaprobe-II, Ulvac) were investigated with $\text{Al K}\alpha$ X-ray at 15 kV. All binding energies were calibrated using the C 1 s line at 284.8 eV. $\text{H}_2\text{-TPR}$ experiments were carried out on Quantachrome ChemBET Pulsar TPR/TPD instrument.

2.4 Catalytic activity measurements

Catalytic activity and stability of the as-prepared Au-CuO/SBA-15 catalysts were evaluated for CO_2 hydrogenation to

methanol by a fixed-bed flow reactor system equipped with stainless steel tube. About 1.0 g (20–40 mesh) fresh catalyst diluted with quartz sand was loaded into the stainless steel tubular reactor, and then pretreated with a mixture of 5 % $\text{H}_2/95$ % Ar under 0.4 MPa at 280°C for 8 h before activity test. Subsequently, the catalyst activity for CO_2 hydrogenation to methanol was tested under the conditions of 250°C, 3 MPa, $n_{(\text{H}_2)}: n_{(\text{CO}_2)} = 3: 1$, $\text{GHSV} = 3600 \text{ h}^{-1}$. After a reaction for 6 h, the exhaust gas and liquid products were analyzed by gas chromatography (Agilent Technologies 6890 USA) equipped with TCD detector for H_2 , CO and CO_2 while FID detector for CH_4 , methanol and other hydrocarbons. The CO_2 conversion and methanol selectivity were calculated by an external normalization method.

3 Results and discussion

3.1 Textural and structural properties

Physicochemical properties of the as-prepared catalysts were summarized in Table 1. The actual Au and Cu contents, measured by ICP-AES, were slightly smaller than their nominal composition. N_2 adsorption–desorption isotherms were presented in Figs. 1 and S1 (see Supplementary Material) respectively. All samples exhibited IV isotherms with a H1-hysteresis loop according to the IUPAC classification, indicating the mesoporous structure wasn't destroyed even after modified with APTES and loaded with Au NPs and CuO NPs.

After introducing $-\text{NH}_2$ groups into SBA-15, the specific surface area (S_{BET}) and pore volume (V_{pore}) decreased significantly while the pore size (D_{pore}) just decreased by 0.8 nm, which indicated that the modifying agent APTES highly dispersed on the inner surface of the channel. The S_{BET} , V_{pore} and D_{pore} of Au/SBA-15 became larger, compared with those of $\text{NH}_2\text{-SBA-15}$. It can be explained that some pore spaces were released when APTES was decomposed during the calcination treatment.

The Au-CuO/SBA-15 also showed a decrease in S_{BET} , V_{pore} and D_{pore} compared with those of bare SBA-15, indicating that Au NPs and CuO NPs were incorporated into the pore channels. The results were also supported by two aspects: (1) the inflection point of the capillary condensation step shifted to lower relative pressure; (2) the hysteresis loop became gradually flat.

Figures 2a and S2 showed low-angle XRD patterns of different samples. All samples showed one major peak (0.9°) and two additional peaks (1.5° and 1.8°), corresponding to the crystal planes of (100), (110) and (200), respectively, which were the typical characteristic of the hexagonal mesostructure with $p6$ mm symmetry in SBA-15. This phenomenon manifested that the mesoscopic

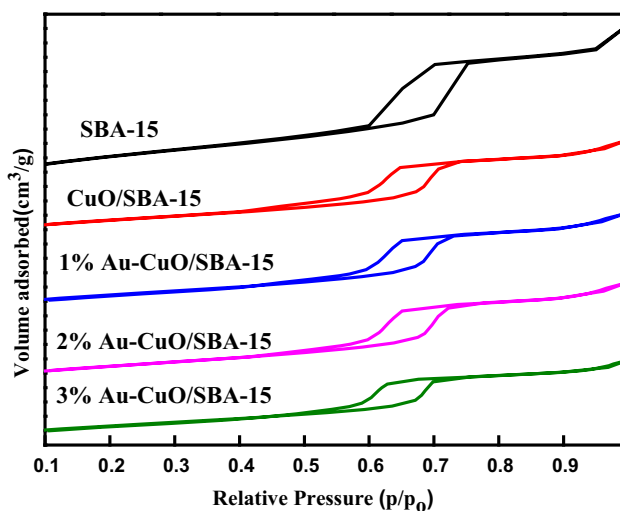
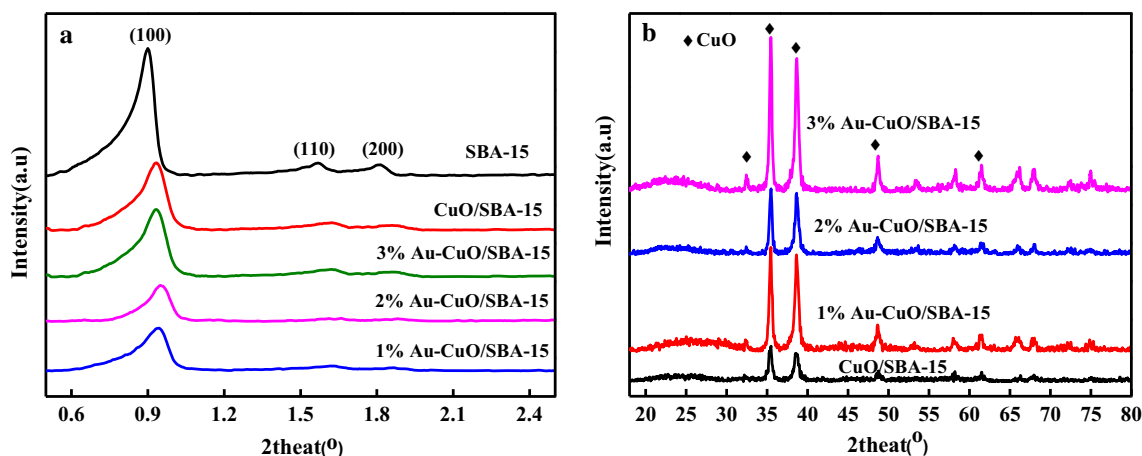
Table 1 Chemical composition and the textural properties of different samples

Sample	Metal loading ^a		d^b_{CuO} (nm)	S_{BET} ($\text{m}^2 \text{g}^{-1}$)	V^c_{pore} ($\text{cm}^3 \text{g}^{-1}$)	D_{pore} (nm)	S_{Cu} ($\text{m}^2 \text{g}^{-1}$)	D_{Cu} (%)
	Au (nm)	Cu (nm)						
SBA-15	–	–	–	560.0	0.878	7.10	–	–
NH_2 -SBA-15	–	–	–	285.1	0.483	6.30	–	–
CuO/SBA-15	–	23.1	10.3	377.4	0.604	5.39	19.7	12.2
1 % Au-CuO/SBA-15	0.92	22.8	13.5	359.4	0.624	5.50	17.0	9.8
2 % Au-CuO/SBA-15	1.79	22.1	11.2	367.4	0.627	5.53	19.2	10.6
3 % Au-CuO/SBA-15	2.76	21.3	17.2	326.6	0.515	5.21	13.2	6.2
2 % Au/SBA-15	1.76	–	–	384.7	0.634	5.81	–	–

^a Metal loading determined by ICP-AES, the nominal Cu loadings was 24 wt%

^b Calculated from XRD patterns using Debye–Scherrer formula

^c Total pore volume obtained from $P/P_0 = 0.99$

**Fig. 1** N_2 adsorption–desorption isotherms of different catalysts**Fig. 2** a The low-angle, b the wide-angle XRD patterns of different samples

ordering was retained after modified with APTES and loaded with Au NPs and CuO NPs. There was a remarkable decrease of the peak intensity after loaded with Au NPs and CuO NPs, illustrating the incorporation of Au NPs and CuO NPs within SBA-15. At the same time, the major peak (100) shifted to higher angle owing to the decrease of d-spacing. Obviously, Au NPs and CuO NPs indeed existed in the channels of SBA-15, as reported elsewhere [26].

Wide-angle XRD patterns of the as-prepared catalysts were presented in Fig. 2b. All samples exhibited diffraction patterns with a broad peak centered at ca. 24° corresponding to amorphous silica walls of SBA-15. For Au/SBA-15, three distinct diffractions at 38.2° , 44.6° and 64.7° for (111), (200) and (220) lattice planes, respectively, confirmed the presence of Au NPs (JCPDS65-2870) (see Fig. S3). The strong diffraction peaks at 32° , 35.4° , 38.6° , 48.7° and 61.3° indicated the presence of CuO NPs

(JCPDS48-1548). No crystalline Au was detected after adding CuO NPs into SBA-15. It should be noted that the actual loading (about 22 wt%) of CuO was so high that Au diffraction peaks were covered by CuO diffraction peaks. As seen in Table 1, the presence of Au NPs had a significant influence on the crystalline size of CuO NPs. The average crystalline size of CuO NPs was in the following order: 3 %Au–CuO/SBA-15(17.2 nm) > 1 %Au–CuO/SBA-15 (13.5 nm) > 2 %Au–CuO/SBA-15 (11.2 nm) > CuO/SBA-15 (10.3 nm). The average crystalline size of CuO NPs increased with the introduction of Au NPs, which suggested that CuO species were agglomerated around Au species and formed large crystallites. However, it can be seen that the crystalline size of CuO NPs in 2 % Au–CuO/SBA-15 was much smaller than that of other Au–CuO/SBA-15. This phenomenon indicated that an appropriate loading amount of Au could improve the thermal ability of the Au–CuO/SBA-15 to inhibit the sintering and aggregation during the heat treatment. The same phenomenon has been observed by other researchers [27, 28].

In order to further investigate the dispersion of CuO NPs, N₂O titration experiments were carried out. S_{Cu} and D_{Cu} were also presented in Table 1. Obviously, the variation tendencies of S_{Cu} and D_{Cu} were correlated well with the average crystalline size of CuO NPs. It can be found that 2 %Au–CuO/SBA-15 showed the maximum S_{Cu} and D_{Cu} about 19.7 m²/g and 12.2 %, respectively. 3 %Au–

CuO/SBA-15 exhibited lowest S_{Cu} and D_{Cu} possibly due to the growth of Au NPs, which would occupy most pores of SBA-15. The fewer pores of SBA-15 led to more CuO NPs aggregated on the external surface of SBA-15.

The representative micrographs of different catalysts were depicted in Figs. 3 and 4. It can be seen that the hexagonal mesostructure of all catalysts was still retained after loaded with Au NPs and CuO NPs, which further confirmed the results of low-angle XRD and N₂ adsorption–desorption. Figure 3a showed that Au NPs were uniformly distributed in the channels and on the surface of SBA-15. The average particle size was about 3.75 nm for Au NPs of 2 % Au/SBA-15. However, both well-dispersed crystalline CuO and aggregated bulk CuO were observed in CuO/SBA-15 (Fig. 3b). The average particle size was about 10.07 nm for dispersed crystalline CuO NPs of CuO/SBA-15. For 2 % Au–CuO/SBA-15, nanoscale metallic particles were highly dispersed on the mesoporous support (Fig. 3c).

The HR-TEM image of 2 % Au–CuO/SBA-15 (Fig. 4) revealed that particles exhibited crystalline structures with d-spacing of 0.235 nm and 0.230 nm corresponding to the (111) plane spacing of Au NPs and CuO NPs, respectively.

According to TEM and HR-TEM images, a schematic illustration of Au/SBA-15 and Au–CuO/SBA-15 can be depicted in Fig. 5. Firstly, Au NPs were highly dispersed on SBA-15 surface. Secondly, CuO NPs were introduced

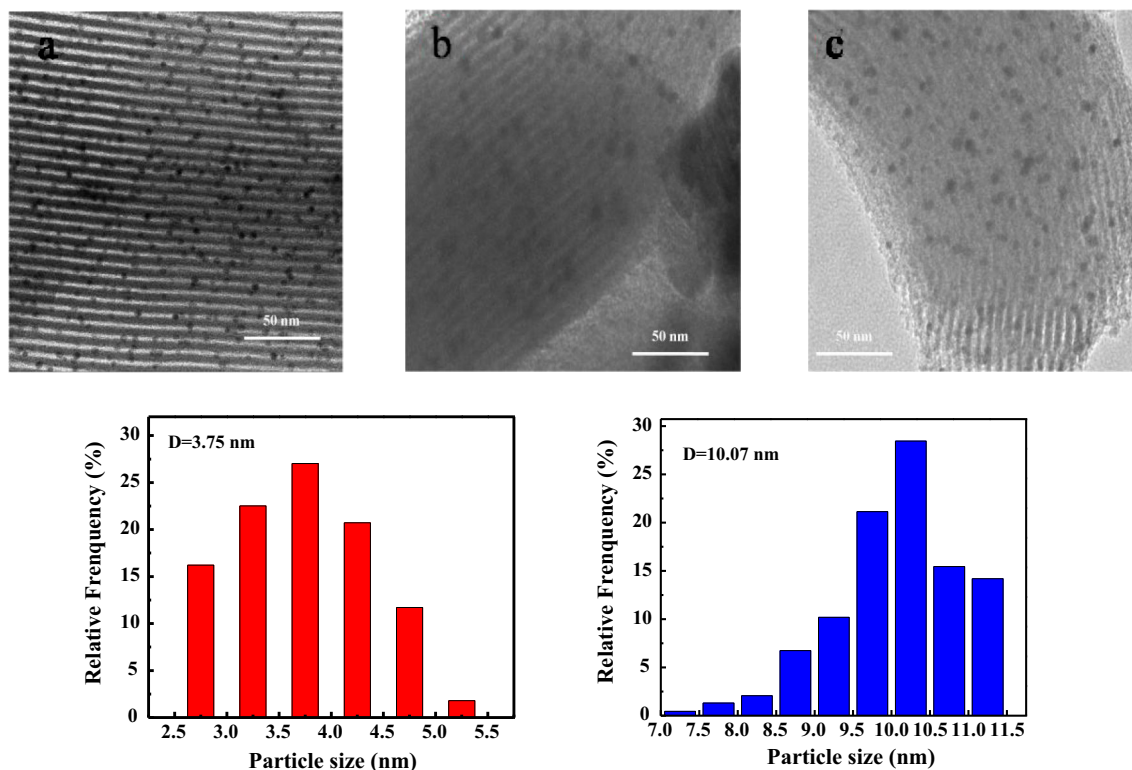


Fig. 3 TEM images of **a** 2 % Au/SBA-15, **b** CuO/SBA-15, **c** 2 % Au–CuO/SBA-15

and agglomerated around Au species during the heat treatment. Finally, the interaction between Au and CuO might be formed, which would be beneficial to enhance the catalytic activity for the hydrogenation of CO₂ to methanol.

3.2 XPS analysis

XPS was employed to determine the surface chemical states of Au and CuO in the catalysts. Several sharp peaks corresponding to Si, O, Au and Cu elements were detected in 2 % Au–CuO/SBA-15 (see Fig. S4). The spectra of Cu 2*p* peaks in CuO/SBA-15 and 2 % Au–CuO/SBA-15 revealed the similar shapes with two main peaks centered at ca. 932.8 (933.1) and 952.8 eV (952.9 eV), along with two satellite peaks at ca. 943 and 963 eV, which can be

assigned to Cu²⁺ 2*p*_{3/2} and 2*p*_{1/2}, respectively (Fig. 6a). The binding energy of Cu 2*p*_{3/2} peak in CuO/SBA-15 shifted to a higher value in comparison with that of 2 % Au–CuO/SBA-15. The phenomenon highlighted the formation of the interaction between Au and CuO. In addition, it has been reported in the literatures that better dispersion of CuO on mesoporous silica may result in a shift of Cu 2*p*_{3/2} peak towards higher binding energy in the CuO-loaded mesoporous silica [29, 30]. It can be also seen from Table 1 that the D_{Cu} and S_{Cu} of CuO/SBA-15 were higher than those of 2 % Au–CuO/SBA-15.

Figure 6b showed typical Au 4*f* XPS peaks for the present catalysts. Two main peaks centered at ca. 83.7 and 87.1 eV in 2 % Au/SBA-15 can be attributed to Au 4*f*_{5/2} and 4*f*_{7/2}, respectively. However, a shift to higher binding energy and the noticeable shoulder peaks were both observed in 2 % Au–CuO/SBA-15. The shift was probably caused by the interaction between Au and CuO. Meanwhile, it was well documented that Au 4*f*_{7/2} signals were featured by peaks at ca. 84.0 eV for Au⁰, ca. 84.6 eV for Au⁺, and ca. 86.0 eV for Au³⁺ [31]. Table 2 showed the contributions of Au species in various chemical states. It can be seen that Au species existed in Au⁰ and Au³⁺. After introducing CuO NPs into Au/SBA-15, the Au species existed in Au⁰, Au⁺ and Au³⁺, which may be related to the electronic interaction between Au and CuO [31].

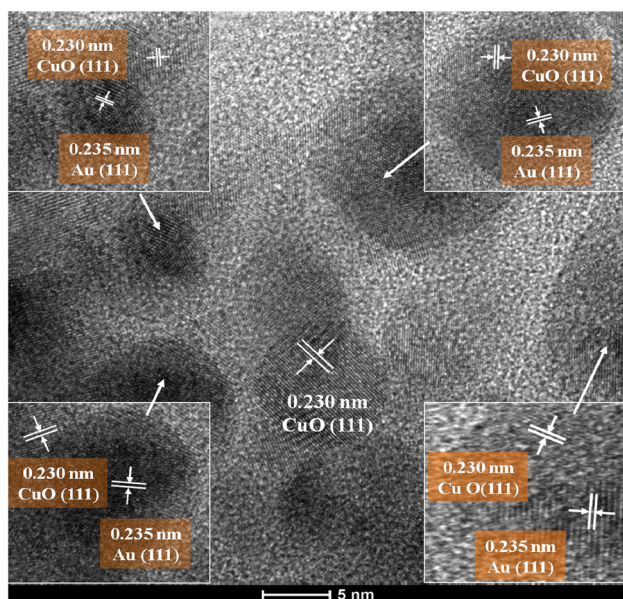
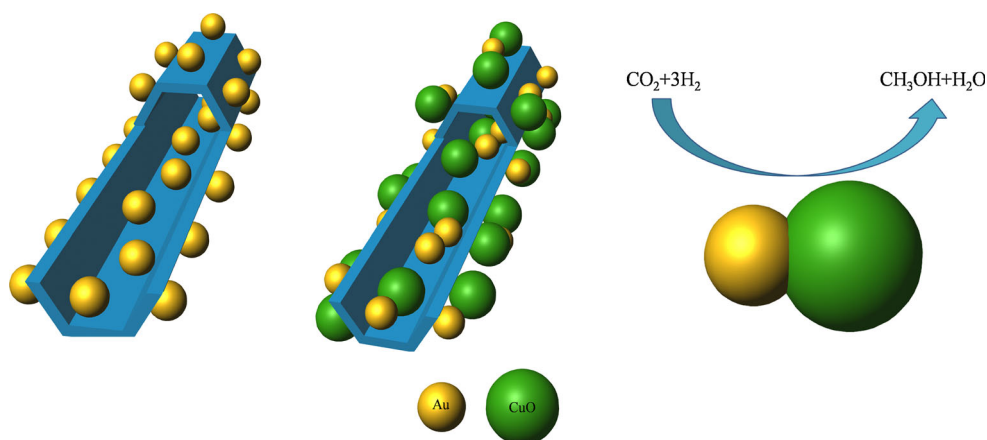


Fig. 4 HR-TEM image of 2 % Au–CuO/SBA-15

Fig. 5 Schematic illustration of CO₂ hydrogenation to methanol over Au–CuO/SBA-15



3.3 H₂-TPR

H₂-TPR was employed to investigate the reduction property of the as-prepared catalysts. It was found that all catalysts exhibited a broad reduction peak below 400°C (Fig. 7). To deeply understand the TPR results, all profiles were fitted into two Gaussian peaks, which were assigned to peak α and peak β, respectively. The former peak was ascribed to the reduction of dispersed CuO species, while the latter was for the reduction of bulk CuO species [32].

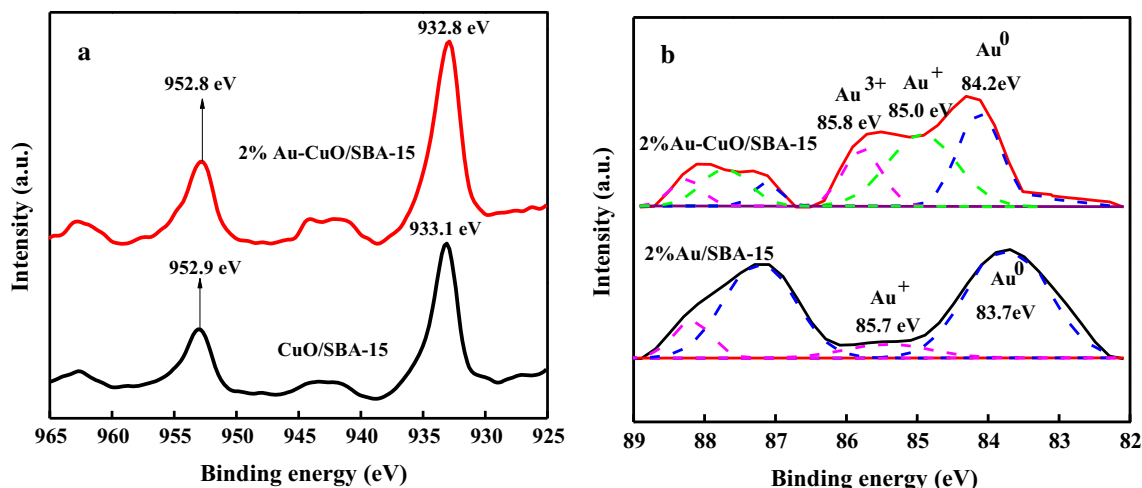


Fig. 6 XPS spectra of **a** Cu 2p in CuO/SBA-15 and 2 % Au–CuO/SBA-15, **b** Au 4f in Au/SBA-15 and 2 % Au–CuO/SBA-15

Table 2 The surface content of different Au chemical states in the catalysts

Catalysts	Au ⁰ (%)	Au ⁺ (%)	Au ³⁺ (%)
2 % Au–CuO/SBA-15	51.4	25.1	23.5
2 % Au/SBA-15	93.6	0	6.4

Table 3 Center of reduction peaks and their contributions to the TPR patterns of the catalysts

Catalysts	T _{max} (°C)		α/(α + β) ^a
	Peak α	Peak β	
CuO/SBA-15	294	335	0.25
1 % Au–CuO/SBA-15	280	328	0.28
2 % Au–CuO/SBA-15	272	318	0.39
3 % Au–CuO/SBA-15	281	326	0.30

^a The contributions of peak α to the TPR patterns

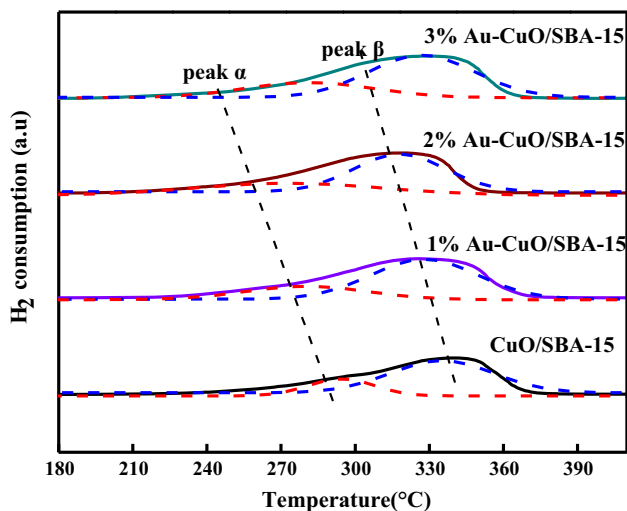


Fig. 7 H₂-TPR profiles of different catalysts

Although the crystallite size of CuO in Au–CuO/SBA-15 was larger than that in CuO/SBA-15, it was worth noting that the peak shifted towards lower temperature compared with that of CuO/SBA-15. This phenomenon demonstrated that the introduction of Au can improve the reducibility of CuO as a consequence of the hydrogen spillover effect at Au/CuO interfaces [33].

Furthermore, it can be seen from Table 3 that the contributions of peak α to the TPR patterns gradually increased

from 0.25 to 0.39 as Au content increased to 2 wt%, owing to the further reduction of CuO through the hydrogen spillover at Au/CuO interfaces [34]. The contributions of peak α to the TPR patterns of 3 % Au–CuO/SBA-15 were lower than those of 2 % Au–CuO/SBA-15, which may result from the presence of larger CuO NPs in 3 % Au–CuO/SBA-15.

3.4 Catalytic activity

Figure 8 summarized the influence of Au content in Au–CuO/SBA-15 on CO₂ conversion and methanol selectivity. The supports and Au/SBA-15 had no catalytic activity for methanol synthesis from CO₂ hydrogenation. Au-containing catalysts exhibited both higher CO₂ conversion and methanol selectivity than CuO/SBA-15. It can be found that 2 % Au–CuO/SBA-15 showed the highest activity with a 24.2 % conversion of CO₂ and 13.5 % selectivity of methanol, owing to stronger interaction between Au and CuO.

As illustrated in Fig. 8a, the CO₂ conversion increased from 15.3 % for CuO/SBA-15 to the maximum 24.2 % for 2 % Au–CuO/SBA-15 and then decreased to 18.4 % for

Fig. 8 The CO₂ conversion and methanol selectivity for CO₂ hydrogenation to methanol over Au–CuO/SBA-15 catalysts (reaction conditions: $n_{\text{H}_2}:n_{\text{CO}_2} = 3:1$, $T = 250^\circ\text{C}$, $P = 3 \text{ MPa}$, $\text{GHSV} = 3600 \text{ h}^{-1}$)

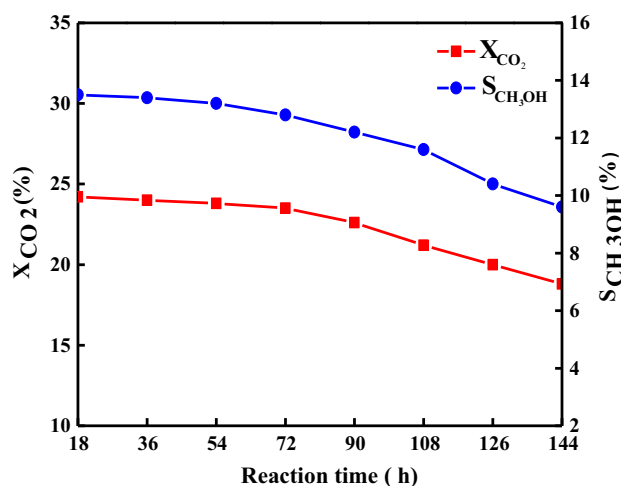
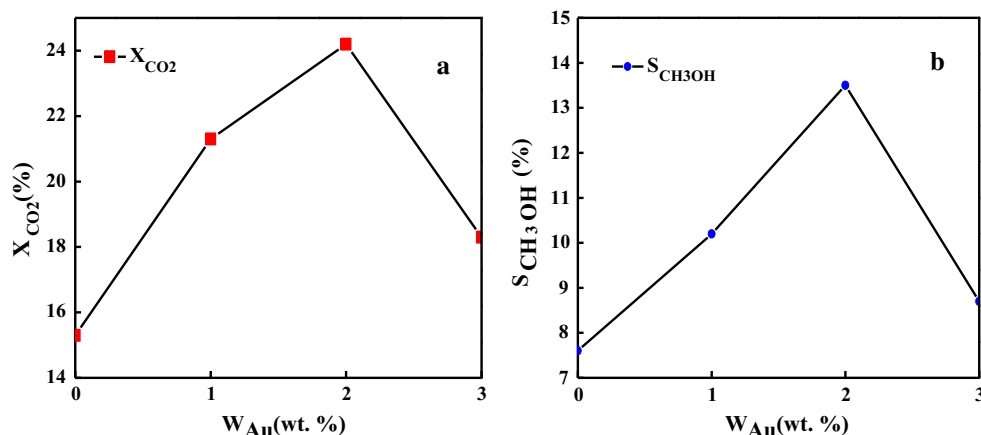


Fig. 9 Stability of 2 % Au–CuO/SBA-15 catalyst for CO₂ hydrogenation to methanol (reaction conditions: $n_{\text{H}_2}:n_{\text{CO}_2} = 3:1$, $T = 250^\circ\text{C}$, $P = 3 \text{ MPa}$, $\text{GHSV} = 3600 \text{ h}^{-1}$)

3 % Au–CuO/SBA-15. It was well-known that S_{Cu} was an important parameter for the catalytic performance of Cu-based catalysts. In general, higher CO₂ conversion was associated with higher S_{Cu} , because that more atomic hydrogen would be produced by dissociative adsorption of H₂ on the active sites of outer copper surface and then would be beneficial for the hydrogenation of the adsorbed carbon containing species [35]. In addition to S_{Cu} , the hydrogen spillover at Au/CuO interfaces, which benefited the reduction of CuO as proved by H₂-TPR results, was responsible for the increase of CO₂ conversion. Therefore, we can better understand the result that CuO/SBA-15 with the largest S_{Cu} and D_{Cu} exhibited the lowest catalytic activity in this view.

The similar variation tendency of methanol selectivity to CO₂ conversion was also observed. The maximum methanol selectivity about 11.5 % was obtained from 2 % Au–CuO/SBA-15 catalyst. As is known to all, the occurrence of RWGS reaction would lead to the decline of

methanol selectivity. Pasupulety et al. [34] found that the introduction of Au NPs into Cu–Zn–Al significantly enhanced the methanol selectivity while slightly improved CO₂ conversion. They attributed this phenomenon to the promotion of the direct CO hydrogenation to methanol ($\text{CO} + 2\text{H}_2 = \text{CH}_3\text{OH}$, $\Delta H_0 = -90.8 \text{ kJ mol}^{-1}$) by Au-containing catalysts in the process of CO₂ hydrogenation to methanol reaction. This conclusion was supported by CO-TPD results, that is, a strong rise in CO release was recorded for Au/Cu–Zn–Al compared with Cu–Zn–Al, suggesting that Au⁰/Au⁺ enhanced the same type of CO adsorption sites like Cu⁰/Cu⁺ in Au/Cu–Zn–Al catalysts. Thus, it can be deduced that the enhancement of methanol selectivity can be attributed to the hydrogen spillover at Au/CuO interfaces, as well as the promotion of direct CO hydrogenation to methanol by Au NPs. Noticeably, 3 % Au–CuO/SBA-15 did not exhibit good catalytic activity. The reason may be attributed to the aggregation of CuO NPs and the coverage of copper active sites by excess Au NPs.

Therefore, it was reasonable to draw the conclusion that the addition of Au NPs played an important role in improving the catalytic activity for the hydrogenation of CO₂ to methanol.

The stability of 2 % Au–CuO/SBA-15 catalyst for methanol synthesis from CO₂ hydrogenation was presented in Fig. 9. It showed that the selectivity of methanol decreased from 13.5 to 9.6 % and the conversion of CO₂ decreased from 24.2 to 18.8 %, respectively, after continuous reaction for 144 h. This phenomenon might be ascribed to the sintering and aggregation of active copper species.

4 Conclusions

Well-dispersed Au–CuO/SBA-15 catalysts with 1–3 wt% Au and 30 wt% CuO were prepared by a two-step process for CO₂ hydrogenation to methanol. The content of Au had

a significant influence on the physicochemical properties and catalytic activity of Au–CuO/SBA-15 catalysts. In the present work, the superior property of the Au–CuO/SBA-15 catalysts can be attributed to the interaction between Au and CuO. Au–CuO/SBA-15 catalysts with a suitable loading amount of Au possessed stronger thermal ability to withstand the sintering and aggregation during the heat treatment; On the other hand, the hydrogen spillover that occurred at Au/CuO interfaces could improve the reducibility of CuO.

Acknowledgments This work was supported by the National Natural Science Foundation of China (Project No. 51404122, 51304099), National Science-technology Support Plan (No. 2011BAC01B03). Also, the authors would like to thank the technical supported from Analysis and Testing Foundation of Kunming University of Science and Technology.

References

1. Y. Chen, S. Choi, L. Thompson, *ACS Catal.* **1717**, 5 (2015)
2. J. Wang, S.M. Lu, J. Li, C. Li, *Chem. Commun.* **17615**, 51 (2015)
3. J. Díez-Ramírez, J.L. Valverde, P. Sánchez, F. Dorado, *Catal. Lett.* **373**, 146 (2016)
4. N. Schuff, *ACS Catal.* **1667**, 2 (2012)
5. J. Kothandaraman, A. Goepfert, M. Czaun, G.A. Olah, G.K.S. Prakash, *J. Am. Chem. Soc.* **778**, 138 (2016)
6. G.A. Olah, *Found. Chem.* **239**, 15 (2013)
7. C. Li, X. Yuan, K. Fujimoto, *Appl. Catal. A Gen.* **306**, 469 (2014)
8. P. Gao, F. Li, N. Zhao, H. Wang, W. Wei, Y.H. Sun, *Acta Phys. Chim. Sin.* **1155**, 30 (2014)
9. H. Ren, C.H. Xu, H.Y. Zhao, Y.X. Wang, J. Liu, J.Y. Liu, *J. Ind. Eng. Chem.* **261**, 28 (2015)
10. H. Ban, C. Li, K. Asami, K. Fujimoto, *Catal. Commun.* **50**, 54 (2014)
11. J. Xiao, D. Mao, X. Guo, J. Yu, *Appl. Surf. Sci.* **146**, 338 (2015)
12. F. Hamdani, H. Abe, B.T. Ovanessian, B. Normand, Y. Watanabe, *RSC Adv.* **2285**, 5 (2015)
13. X. Dong, F. Li, N. Zhao, F.K. Xiao, J.W. Wang, Y.S. Tan, *Appl. Catal. B* **8**, 191 (2016)
14. Y. Hartadi, D. Widmann, R.J. Behm, *Phys. Chem. Chem. Phys.* **10781**, 18 (2016)
15. Y. Hartadi, D. Widmann, R.J. Behm, *J. Catal.* **238**, 333 (2016)
16. Y. Hartadi, D. Widmann, R.J. Behm, *ChemSusChem* **456**, 8 (2014)
17. P. Mierczynski, T.P. Maniecki, W. Maniukiewicz, W.K. Jozwiak, *React. Kinet. Mech. Catal.* **139**, 104 (2011)
18. H. Sakurai, M. Haruta, *Catal. Today* **361**, 29 (1996)
19. S. Sareen, V. Mutreja, S. Singh, B. Pal, *RSC Adv.* **184**, 5 (2014)
20. C.S. Chen, Y.T. Lai, T.W. Lai, J.H. Wu, C.H. Chen, J.F. Lee, H.M. Kao, *ACS Catal.* **217**, 3 (2013)
21. S. Sareen, V. Mutreja, B. Pal, S. Singh, *Microporous Mesoporous Mater.* **219**, 202 (2015)
22. X. Liu, A. Wang, X. Wang, C.Y. Mou, T. Zhang, *Chem. Commun.* **3187**, 27 (2008)
23. D. Zhao, I. Feng, Q. Huo, N. Melosh, G.H. Fredrickson, B.F. Chmelka, G.D. Stucky, *Science* **548**, 279 (1998)
24. T.K. Pathak, V. Kumar, J. Prakash, L.P. Purohit, H.C. Swart, R.E. Kroon, *Sens. Actuators A* **247**, 475 (2016)
25. H. Lei, Z. Hou, J. Xie, *Fuel* **191**, 164 (2016)
26. T. Wang, X. Yuan, S. Li, L. Zeng, J. Gong, *Nanoscale* **7593**, 7 (2015)
27. J.W. Lee, X. Liu, C.Y. Mou, *J. Chin. Chem. Soc.* **907**, 60 (2013)
28. X.Y. Liu, A.Q. Wang, T. Zhang, D.S. Su, C.Y. Mou, *Catal. Today* **103**, 160 (2011)
29. J. Czaplinska, I. Sobczak, M. Ziolk, *J. Phys. Chem. C* **12796**, 118 (2014)
30. A.G. Kong, H.W. Wang, X. Yang, Y.W. Hou, Y.K. Shan, *Microporous Mesoporous Mater.* **348**, 118 (2009)
31. T. Tian, Y. Liu, X.G. Zhang, *Chin. J. Catal.* **1358**, 36 (2015)
32. H. Lei, R.F. Nie, G.Q. Wu, Z.Y. Hou, *Fuel* **161**, 154 (2015)
33. C. Kartusch, J.A. Bokhoven, *Gold Bull.* **343**, 42 (2009)
34. N. Pasupulety, H. Driss, Y.A. Alhamed, A.A. Alzahrani, M.A. Daous, L. Petrov, *C. R. Acad. Bulg. Sci.* **1511**, 68 (2015)
35. P. Gao, F. Li, H.J. Zhan, N. Zhao, F.K. Xiao, W. Wei, L.S. Zhong, H. Wang, Y.H. Sun, *J. Catal.* **51**, 298 (2013)